

Interface correlated exchange bias effect in epitaxial Fe_3O_4 thin films grown on SrTiO_3 substrates

Cite as: Appl. Phys. Lett. **105**, 241604 (2014); <https://doi.org/10.1063/1.4904471>

Submitted: 11 September 2014 . Accepted: 06 December 2014 . Published Online: 16 December 2014

Qiu-Xiang Zhu, Ming Zheng, Ming-Min Yang, Ren-Kui Zheng, Yu Wang, Xiao-Min Li, and Xun Shi



View Online



Export Citation



CrossMark

ARTICLES YOU MAY BE INTERESTED IN

[Room temperature in-plane \$\langle 100 \rangle\$ magnetic easy axis for \$\text{Fe}_3\text{O}_4/\text{SrTiO}_3\(001\):\text{Nb}\$ grown by infrared pulsed laser deposition](#)

Journal of Applied Physics **114**, 223902 (2013); <https://doi.org/10.1063/1.4837656>

[Unconventional magnetization of \$\text{Fe}_3\text{O}_4\$ thin film grown on amorphous \$\text{SiO}_2\$ substrate](#)

AIP Advances **6**, 065111 (2016); <https://doi.org/10.1063/1.4954035>

[Investigation on the origin of exchange bias in epitaxial, oriented and polycrystalline \$\text{Fe}_3\text{O}_4\$ thin films](#)

AIP Advances **5**, 117123 (2015); <https://doi.org/10.1063/1.4935787>

Lock-in Amplifiers
Find out more today



Zurich
Instruments

AIP
Publishing

Interface correlated exchange bias effect in epitaxial Fe₃O₄ thin films grown on SrTiO₃ substrates

Qiu-Xiang Zhu,¹ Ming Zheng,¹ Ming-Min Yang,¹ Ren-Kui Zheng,^{1,a)} Yu Wang,² Xiao-Min Li,^{1,b)} and Xun Shi¹

¹State Key Laboratory of High Performance Ceramics and Superfine Microstructure, Shanghai Institute of Ceramics, Chinese Academy of Sciences, Shanghai 200050, China

²Department of Applied Physics and Materials Research Center, The Hong Kong Polytechnic University, Hong Kong, China

(Received 11 September 2014; accepted 6 December 2014; published online 16 December 2014)

We report exchange bias effect in Fe₃O₄ films epitaxially grown on SrTiO₃ substrates. This effect is related to the formation of Ti³⁺-vacancy complexes at the surface of SrTiO₃ in ultrahigh vacuum that in turn triggers the growth of a thin antiferromagnetic (AFM) FeO layer (~5 nm) at the interface. The picture of antiferromagnetic FeO interacting with native ferrimagnetic Fe₃O₄ matrix reasonably accounts for this anomalous magnetic behavior. With increasing film thickness from 17 to 43 nm, the exchange bias effect and the magnetization anomaly associated with the AFM phase transition of the FeO layer are progressively weakened due to the increase in the volume fraction of the Fe₃O₄ phase, indicating the interfacial nature of the exchange coupling. Our results highlight the important role of interface engineering in controlling the magnetic properties of iron oxide thin films. © 2014 AIP Publishing LLC. [<http://dx.doi.org/10.1063/1.4904471>]

Chemical and physical interactions at artificial heterointerface could lead to exotic and unexpected physical properties and functionalities, such as interface superconductivity, magnetoelectric coupling, orbital reconstruction, exchange bias, and quantum Hall effect.^{1–3} Among these emergent phenomena, the exchange bias is fascinating for its rich underlying physics and various potential applications, ranging from spintronic devices and spin valves to magnetic tunnel junctions.^{4–6} The exchange coupling across the interface between two materials with competing magnetic interactions is frequently manifested in the form of horizontal shift in the magnetic hysteresis loop accompanied by an increase in coercivity after cooling samples in a magnetic field.⁷ A model system for this study is iron oxides, among which the Fe₃O₄ is ferrimagnetic (FIM), while the FeO (wüstite) is antiferromagnetic (AFM). Great endeavor has been devoted to the synthesis of multicomponent core-shell structured nanoparticles (e.g., FeO/Fe₃O₄) with the aim of improving and tuning their magnetic properties.^{8–11} Exploiting the formation of antiferromagnetic FeO and its subsequent oxidation in air has enabled the study of the exchange bias of the FeO/Fe₃O₄ core-shell nanostructures, promoting a better understanding of the exchange bias effect at the nanoscale level. Previous works on FeO/Fe₃O₄ systems with AFM/FIM interface are mainly limited to zero-dimensional (0D) structures. Hence, it is much meaningful to extend this concept to other configurations such as two-dimensional (2D) heterostructures.

Here, we report the fabrication and characterization of 2D iron oxide films with exchange bias effect. Compared with the 0D FeO/Fe₃O₄ core-shell nanostructure based devices, the utilization of 2D thin-film structure would be

beneficial in terms of increasing device reproducibility and reducing the fabrication cost in light of the mature thin-film fabrication technology. Additionally, exchange bias is most commonly studied in thin-film structures that facilitate the integration and patterning of devices for technological applications.¹² In this paper, we demonstrate how interfacial effect can induce specific phase through precisely controlling the growth condition, which is nowadays extensively recognized as key for the design of diverse devices with tailored functionalities. Consequently, exchange bias emerges in seemingly single-phase Fe₃O₄ systems by interface engineering.

Fe₃O₄ thin-film samples with thickness ranging from 17 to 43 nm were grown on (001)-oriented SrTiO₃ single-crystal substrates by ablating a high purity Fe₂O₃ ceramic target using pulsed laser ($\lambda = 248$ nm), which was *in situ* monitored by reflection high-energy electron diffraction. Film deposition was carried out at a substrate temperature of 400 °C under high vacuum ($<3 \times 10^{-4}$ Pa), with the rotation of sample holder in order to avoid compositional dispersion over the sample. After deposition, the samples were *in situ* cooled to room temperature. For a comparison with the Fe₃O₄/SrTiO₃(001) structure, we also prepared the Fe₃O₄/0.72Pb(Mg_{1/3}Nb_{2/3})O₃-0.28PbTiO₃ (PMN-PT)(001) and Fe₃O₄/MgAl₂O₄(001) structures with and without a SrTiO₃ buffer layer (~10 nm) under identical conditions. The growth conditions of the SrTiO₃ layer are 700 °C, 0.01 Pa and 7 J/cm² for substrate temperature, oxygen pressure, and pulse energy density, respectively.

The film thickness and composition were measured using a FEI Magellan 400 scanning electron microscope (SEM), attached with an energy-dispersive x-ray spectrometer (EDS). Meanwhile, the electron-back scatter diffraction (EBSD) was conducted on a FEI dual beam workstation (Strata DB 235) equipped with a TSL OIM analysis unit. The Kikuchi patterns were generated at an acceleration voltage of 5 kV and recorded by a DigiView camera system.

a) zrk@ustc.edu

b) lixm@mail.sic.ac.cn

The crystal structures of the samples were characterized by a high resolution Bruker D8 Discover x-ray diffractometer equipped with Cu $K_{\alpha 1}$ radiation ($K_{\alpha 1} = 1.5406 \text{ \AA}$) and Tecnai G2 F20 S-Twin transmission electron microscope (TEM).

The temperature dependence of the resistance under magnetic fields was measured by a Physical Property Measurement System (PPMS-9, Quantum Design). The magnetic property measurements were carried out on a superconducting quantum interference device (MPMS XL-5, Quantum Design) magnetometer, with the magnetic field applied in the film plane. Note that the diamagnetic contribution from the substrates has been subtracted from the magnetization raw data.

Figure 1(a) shows the temperature dependence of the resistance for the Fe_3O_4 (26 nm)/ $\text{SrTiO}_3(001)$ structure. The resistance of the film increases with decreasing temperature and undergoes an unobvious transition (i.e., the Verwey transition) near $T_V \sim 108 \text{ K}$, suggesting a high density of anti-phase boundaries (APBs) in the film which also accounts for the deviation of T_V from bulk values ($T_V \sim 120 \text{ K}$). Using high resolution x-ray and neutron powder diffraction, Wright *et al.* elucidated that the Verwey transition with a sharp resistance change occurs only when the Fe^{2+} and Fe^{3+} ions at the octahedral sites form long range ordering.¹³ Indeed, these octahedral coordinated Fe^{2+} and Fe^{3+} ions involve in the electron conduction process, i.e., thermally activated hopping of electrons between the Fe^{2+} and Fe^{3+} ions. The interruption of the long range ordering of the Fe^{2+} and Fe^{3+} ions across the natural growth related defects (e.g., the APBs) would modify the electron hopping amplitude and the magnetic interactions between neighboring Fe ions. Eerenstein *et al.*¹⁴ and Moussy *et al.*¹⁵ reported that the Verwey transition was suppressed with decreasing film thickness, due to the increase in the density of APBs. The inset of Fig. 1(a)

shows the temperature dependence of magnetoresistance (MR) under a magnetic field of $H = 9 \text{ T}$ for the Fe_3O_4 film. Here, $MR = \Delta R/R = [R(0T) - R(9T)]/R(0T)$. Upon decreasing temperature from 300 K , $\Delta R[\Delta R = R(0T) - R(9T)]$ increases continuously from $\sim 10^2 \Omega$ at 300 K to $\sim 10^5 \Omega$ at 90 K , approximately three orders of change in ΔR . However, $\Delta R/R$ has a maximum value ($\sim 8.4\%$) at $T \sim 108 \text{ K}$, close to T_V , indicating that the electronic transport is maximally sensitive to the magnetic field near the Verwey transition. Fig. 1(b) displays the zero-field-cooled (ZFC) and field-cooled (FC) magnetization of the Fe_3O_4 film as a function of temperature, as measured with the magnetic field ($H = 500 \text{ Oe}$) applied in the film plane. With increasing temperature, the upturns in both ZFC and FC curves originated from the Verwey transition of the Fe_3O_4 were quantitatively determined to be 108 K from the first derivative of magnetization versus temperature [inset of Fig. 1(b)], consistent with the resistance measurements in Fig. 1(a). In addition, with increasing temperature there is a noticeable increase in the magnetization at 192 K in the ZFC case, in proximity to the Néel temperature of the FeO ($\sim 200 \text{ K}$),¹⁰ implying the presence of the AFM FeO phase in the film. Fig. 1(c) shows the magnetization-magnetic field (M - H) hysteresis loops for the $\text{Fe}_3\text{O}_4(26 \text{ nm})/\text{SrTiO}_3$ structure, which were measured at 10 K after being cooled from 300 K with and without the application of $H = 1 \text{ T}$ or -1 T in-plane magnetic field. Remarkably, the ZFC M - H curve shows a coercive field (H_C) of 385 Oe , and shifts toward negative field by an exchange bias field (H_{EB}) of 235 Oe , since the cooling starts from a remanent state.¹⁶ The M - H curve intersects the H -axis at two points, i.e., H_L and H_R . H_C and H_{EB} are defined as $H_C = |H_L - H_R|/2$ and $H_{EB} = |H_L + H_R|/2$, respectively. For the FC M - H curves, there is a shift of 360 Oe towards the opposite direction of the cooling field along the H -axis,

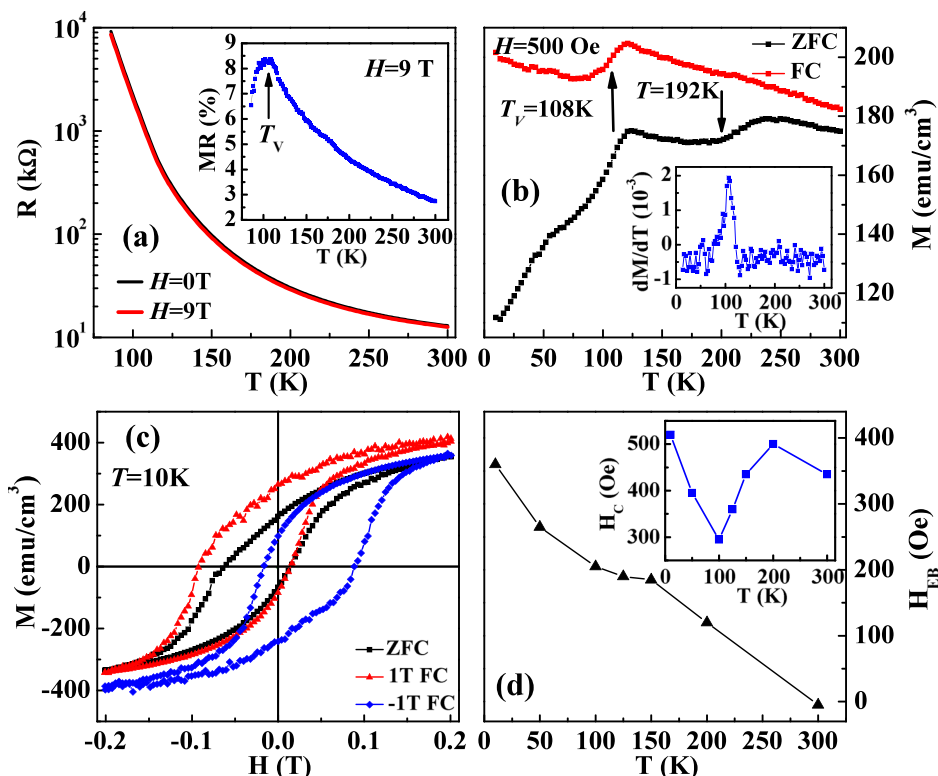


FIG. 1. Electrical and magnetic properties of the Fe_3O_4 (26 nm)/ SrTiO_3 structure. (a) Temperature dependence of the resistance under $H = 0$ and 9 T . Inset: MR versus T curve. (b) ZFC and FC magnetization versus T , as measured with $H = 500 \text{ Oe}$ applied in the film plane. dM/dT versus T for FC magnetization. (c) M - H hysteresis loops at $T = 10 \text{ K}$. (d) Temperature dependence of the exchange bias field when the film was cooled under $H = -1 \text{ T}$. The inset shows the temperature dependence of the coercivity.

accompanied by an enhancement of coercivity, which is the typical fingerprint of exchange bias. Moreover, there is obvious vertical shift in the M - H loops for the FC conditions. The vertical shift in M - H loop is commonly observed in exchange coupled FeO/Fe₃O₄ core-shell nanoparticle systems and can be explained by the presence of uncompensated spins at the AFM/FIM interface.¹⁰ As can be seen from Fig. 1(d) and the inset, the exchange bias field decreases with the rise of temperature and the coercive field shows a minimum near the Verwey transition. It's worthy to point out that we have measured the M - H curves of the Fe₃O₄ film in different magnetic fields and found that the saturation in the magnetization can be hardly reached, even in fields as large as 1 T, probably originated from the antiphase boundary¹⁵ and AFM FeO phase within the films.

Intriguingly, exchange bias effect in Fe₃O₄/PMN-PT(001) and Fe₃O₄/MgAl₂O₄(001) structures is minor and neglectable. However, this effect can be enhanced significantly by the insertion of a thin SrTiO₃ layer between the Fe₃O₄ layer and the substrates (see Fig. S1 of the supplementary material¹⁷), which hints that the SrTiO₃ plays a key role in determining the magnetic properties of iron oxide films. Indeed, a weak exchange bias effect ($H_{EB} = 52$ Oe) has been observed in Fe₃O₄ thin films and was exclusively due to the formation of APBs in the film.¹⁸ Also, APBs were believed to be responsible for small H_{EB} (~ 50 – 126 Oe) in pure Fe₃O₄ nanoparticles prepared by a seeded-growth method.^{19,20} Such large exchange bias effect ($H_{EB} = 360$ Oe) is unprecedented in our two-dimensional iron oxide system and can be understood not simply on the basis of the APBs picture, but from the microstructural point of view. We thus conducted the x-ray

diffraction (XRD) θ - 2θ scan, EBSD, cross-sectional SEM, and high resolution TEM measurements on the Fe₃O₄(26 nm)/SrTiO₃ sample. The XRD θ - 2θ scan pattern in Fig. 2(a) demonstrates that the Fe₃O₄ film exhibits c -axis preferential orientation on the SrTiO₃(001) substrate. Using the EBSD technique, we further identified the crystallographic orientation of the film. The insets (a) and (b) of Fig. S2 of the supplementary material¹⁷ present the EBSD Kikuchi patterns and the corresponding indexation for the film, which was obtained by scanning electron beam over the film surface and were indexed and analyzed automatically by means of software. The structure is analyzed to be magnetite, and the resulting crystallographic orientation is determined to be [001] via the Eulerian angles given below the indexed pattern. The cross-sectional SEM image [Fig. 2(b)] shows that the film has a dense microstructure with a thickness of 26 nm. In Fig. 2(c) we present the selected area electron diffraction (SAED) patterns, taken with the electron beam parallel to the [0-44] direction of Fe₃O₄ film. The diffraction spots correspond to the SrTiO₃ substrate and the Fe₃O₄ film, respectively. The relative orientation of the film with respect to the substrate is [400]Fe₃O₄//[200]SrTiO₃ and [0-44]Fe₃O₄//[0-22]SrTiO₃. The high resolution TEM image in Fig. 2(d) shows that the interface between the substrate and the film is atomically sharp. However, what is unexpected is that a thin layer of FeO phase (~ 5 nm) with a clear lattice fringe and a lattice spacing of 0.212 nm for the (200) plane appears near the interface. While the lattice fringes of Fe₃O₄ phase with a lattice spacing of 0.294 nm for the (220) plane can be found throughout the film. Note that EDS measurements (see Fig. S2 of the supplementary

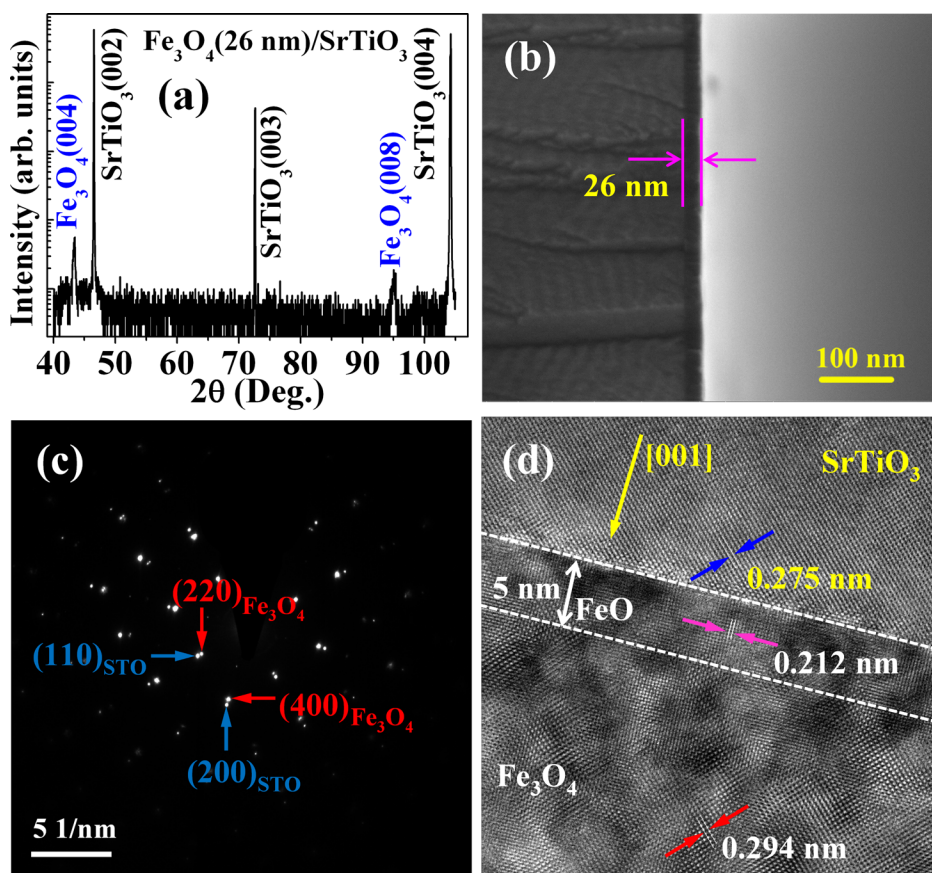


FIG. 2. XRD and microstructural characterization of the Fe₃O₄(26 nm)/SrTiO₃ structure. (a) XRD θ - 2θ scan pattern. (b) Cross-sectional SEM image. (c) SAED pattern recorded from the area covering both the film and the substrate along the [0-44] zone axis of the Fe₃O₄ film. The diffraction spots are indexed with magnetite and SrTiO₃. (d) HRTEM image taken at the interface.

material¹⁷) on the surface of the film show that the relative content ratios of Fe and O is approximately 0.75, confirming the stoichiometry of the Fe_3O_4 upper layer. Such lattice structure could be related to the particular sample preparation conditions. Before deposition, the SrTiO_3 substrates were annealed at 400°C under high vacuum with the base pressure less than 3×10^{-4} Pa for more than 1 h. Annealing the SrTiO_3 in high vacuum would result in oxygen loss and the formation of so called Ti^{3+} -oxygen vacancy complexes at the upmost surface.²¹ The growth thermodynamic landscape of the iron oxides is thus strongly influenced by these interface defects. Specifically, during the initial growth stage of the Fe_3O_4 , the highly reactive Ti^{3+} ions at the surface were readily reoxidised to Ti^{4+} ions by reacting with the oxygen atoms of the Fe_3O_4 . Consequently, a thin FeO layer appears at the interface, which has a great impact on the exchange bias.

On the basis of the above structural analysis, we attribute the exotic magnetic behavior of the $\text{Fe}_3\text{O}_4/\text{SrTiO}_3$ sample to the AFM/FIM exchange coupling due to the appearance of the FeO phase at the interface. In the classical phenomenological picture, when samples are cooled in an external magnetic field from above the Néel temperature, the interfacial uncompensated spins of the AFM phase are oriented along or opposite to the FM phase magnetization, depending on the interfacial exchange energy. The AFM phase acts as a pinning layer, leading to a unidirectional anisotropy or a preferred orientation of the magnetization in the FM layer. In other words, it is more difficult to switch the magnetization of the FM in the direction opposite to the cooling field direction than it is to switch it back to the cooling field direction, manifested as a shift in the M - H loop along the H -axis. Besides, under the circumstance of positive (negative) field cooling (i.e., $H = +1$ T or -1 T), the negative (positive) maximal magnetization is approximately the same as that for the ZFC condition, whereas the positive (negative) maximal magnetization is much larger than that for the ZFC condition [see Fig. 1(c)], further confirming the preferential alignment of the uncompensated interfacial spins in the field cooled case.

To get a better insight into the magnetic properties of the $\text{Fe}_3\text{O}_4/\text{SrTiO}_3$ structure, we fabricated a series of $\text{Fe}_3\text{O}_4/\text{SrTiO}_3$ structures with different film thicknesses by controlling deposition time. Fig. 3 presents the ZFC and FC magnetization versus temperature (T) curves. As the film thickness increases, the M - T curves display typical feature of Fe_3O_4 with the Verwey transition much more prominent and the magnetic anomalies (i.e., the upturn of the magnetization above 192 K) associated with the phase transition of the FeO was progressively weakened. For thick films (35 and 43 nm), both the ZFC and FC M - T curves exhibit a maximal magnetic moment at 125 K, which is defined as the blocking temperature (T_B). At this temperature, the energy of the aligned magnetic moments is balanced with the thermal energy. Above this temperature thermal perturbation destroys the alignment of the moments. Below T_B , the magnetization shows a gradual increase with increasing temperature as the moments progressively reorient along the field direction at low temperatures (10–125 K), whereas the FC curve displays a flat line at low temperature because of the saturation of the magnetic moments. Note that similar magnetic behaviors

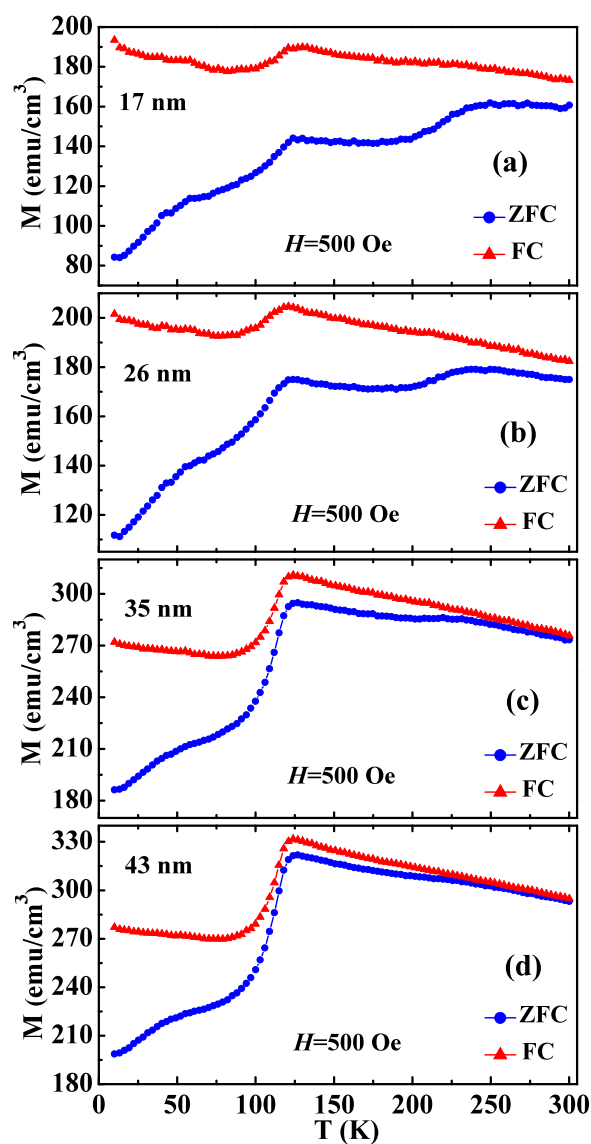


FIG. 3. Temperature dependence of the ZFC and FC magnetization for the $\text{Fe}_3\text{O}_4/\text{SrTiO}_3$ structures with different film thicknesses (a) 17 nm, (b) 26 nm, (c) 35 nm, and (d) 43 nm.

have been observed in literatures pertaining to magnetite nanowires.²² Overall, the M - T profiles highlight that with increasing film thickness the volume fraction of the Fe_3O_4 phase increases, resulting in increasing contribution of the Fe_3O_4 to the magnetization.

Figure 4 depicts the selected M - H loops at 10 K in the positive and negative field cooled conditions. It is evident that the shape and position of the M - H loops vary considerably with film thickness. For the 17 nm thick sample, both prominent vertical and horizontal displacement of the hysteresis loop can be identified for FC conditions. The horizontal shift is so large that both the descending and ascending coercive fields are almost of the same sign. With increasing film thickness, exchange bias effect is suppressed significantly, confirming the increasing (decreasing) volume fraction of the Fe_3O_4 (FeO) phase, since the magnitude of the exchange bias directly correlates to the number of uncompensated interfacial spins that are pinned to the antiferromagnet.²³ For thick films, the unpinned spins increase and can be reversed more easily upon the switch of external field direction.

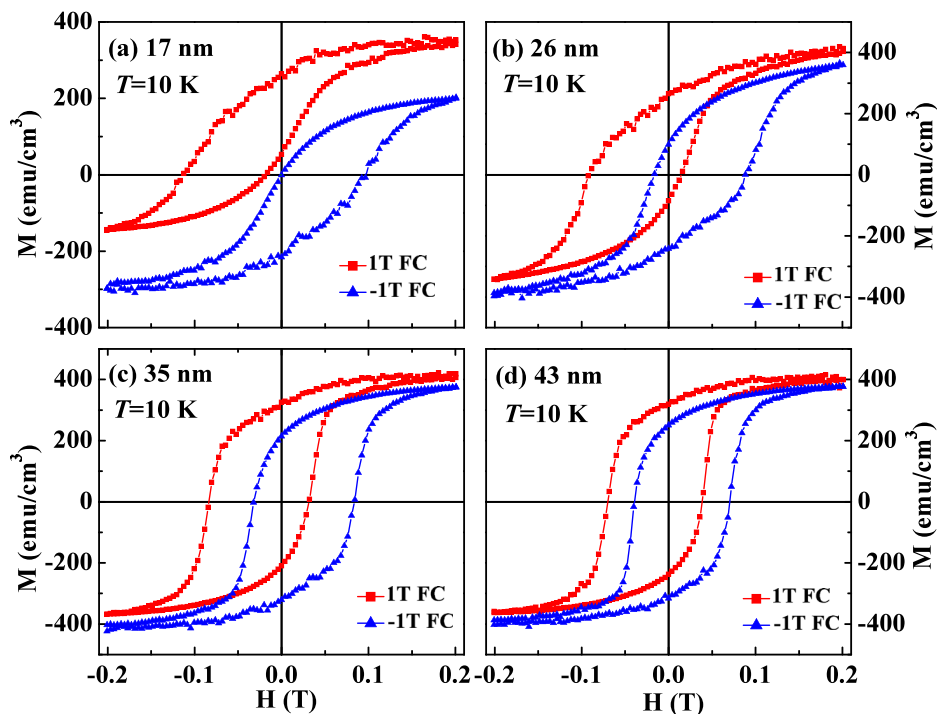


FIG. 4. M - H hysteresis loops measured at 10 K after the $\text{Fe}_3\text{O}_4/\text{SrTiO}_3$ samples with different film thicknesses were cooled to 10 K under $H=1\text{ T}$ and -1 T , respectively, (a) 17 nm, (b) 26 nm, (c) 35 nm, and (d) 43 nm.

In summary, we report exchange bias effect in $\text{Fe}_3\text{O}_4/\text{SrTiO}_3$, $\text{Fe}_3\text{O}_4/\text{SrTiO}_3/\text{PMN-PT}$, $\text{Fe}_3\text{O}_4/\text{SrTiO}_3/\text{MgAl}_2\text{O}_4$ structures through a serial study of Fe_3O_4 films on SrTiO_3 , PMN-PT , and MgAl_2O_4 substrates. The reduction of SrTiO_3 surface in ultrahigh vacuum results in an interfacial monolayer consisting of FeO with subsequent growth of epitaxial Fe_3O_4 layer. Thus, the exchange bias effect can be plausibly understood in the framework of exchange coupling between the AFM FeO with the FIM Fe_3O_4 . For the $\text{Fe}_3\text{O}_4/\text{SrTiO}_3$ structures, with increasing total thickness of the film, the magnetization anomaly associated with the AFM phase transition of the FeO is gradually smeared out due to the decreasing magnetic contribution from the FeO and the exchange bias effect is progressively weakened, implying the interfacial nature of the exchange coupling. The demonstration of exchange bias in 2D iron oxide film manifests the important role of interface engineering in tailoring the magnetic properties of iron oxide films.

This work was supported by the Natural National Science Foundation of China (Grant Nos. 51172259, 51428202, and 11090332) and the CAS/SAFEA International Partnership Program for Creative Research Teams.

¹N. Reyren, S. Thiel, A. D. Caviglia, L. F. Kourkoutis, G. Hammer, C. Richter, C. W. Schneider, T. Kopp, A. S. Ruetschi, D. Jaccard, M. Gabay, D. A. Muller, J. M. Triscone, and J. Mannhart, *Science* **317**, 1196 (2007).

²H. Y. Hwang, Y. Iwasa, M. Kawasaki, B. Keimer, N. Nagaosa, and Y. Tokura, *Nat. Mater.* **11**, 103 (2012).

³P. Yu, Y.-H. Chu, and R. Ramesh, *Mater. Today* **15**, 320 (2012).

⁴A. A. Tulapurkar, Y. Suzuki, A. Fukushima, H. Kubota, H. Maehara, K. Tsunekawa, D. D. Djayaprawira, N. Watanabe, and S. Yuasa, *Nature* **438**, 339 (2005).

⁵J. C. S. Kools, *IEEE Trans. Magn.* **32**, 3165 (1996).

⁶Y. Jiang, T. Nozaki, S. Abe, T. Ochiai, A. Hirohata, N. Tezuka, and K. Inomata, *Nat. Mater.* **3**, 361 (2004).

⁷J. Nogues and I. K. Schuller, *J. Magn. Magn. Mater.* **192**, 203 (1999).

⁸B. P. Pichon, O. Gerber, C. Lefevre, I. Florea, S. Fleutot, W. Baaziz, M. Pauly, M. Ohlmann, C. Ulhaq, O. Ersen, V. Pierron-Bohnes, P. Panissod, M. Drillon, and S. Begin-Colin, *Chem. Mater.* **23**, 2886 (2011).

⁹E. Wetterskog, C. W. Tai, J. Grins, L. Bergstrom, and G. Salazar-Alvarez, *ACS Nano* **7**, 7132 (2013).

¹⁰X. L. Sun, N. F. Huls, A. Sigdel, and S. H. Sun, *Nano Lett.* **12**, 246 (2012).

¹¹D. W. Kavich, J. H. Dickerson, S. V. Mahajan, S. A. Hasan, and J. H. Park, *Phys. Rev. B* **78**, 174414 (2008).

¹²M. Bibes, J. E. Villegas, and A. Barthelemy, *Adv. Phys.* **60**, 5 (2011).

¹³J. P. Wright, J. P. Attfield, and P. G. Radaelli, *Phys. Rev. Lett.* **87**, 266401 (2001).

¹⁴W. Eerenstein, T. T. M. Palstra, T. Hibma, and S. Celotto, *Phys. Rev. B* **66**, 201101(R) (2002).

¹⁵J. B. Moussy, S. Gota, A. Bataille, M. J. Guittet, M. Gautier-Soyer, F. Delille, B. Dieny, F. Ott, T. D. Doan, P. Warin, P. Bayle-Guillemaud, C. Gatel, and E. Snoeck, *Phys. Rev. B* **70**, 174448 (2004).

¹⁶P. Miltenyi, M. Gierlings, M. Bammig, U. May, G. Guntherodt, J. Nogues, M. Gruyters, C. Leighton, and I. K. Schuller, *Appl. Phys. Lett.* **75**, 2304 (1999).

¹⁷See supplementary material at <http://dx.doi.org/10.1063/1.4904471> for Figs. S1 and S2.

¹⁸S. K. Arora, R. G. S. Sofin, A. Nolan, and I. V. Shvets, *J. Magn. Magn. Mater.* **286**, 463 (2005).

¹⁹A. Espinosa, A. Munoz-Noval, M. Garcia-Hernandez, A. Serrano, J. J. de la Morena, A. Figuerola, A. Quarta, T. Pellegrino, C. Wilhelm, and M. A. Garcia, *J. Nanopart. Res.* **15**, 1514 (2013).

²⁰M. Levy, A. Quarta, A. Espinosa, A. Figuerola, C. Wilhelm, M. Garcia-Hernandez, A. Genovese, A. Falqui, D. Alloyeau, R. Buonsanti, P. D. Cozzoli, M. A. Garcia, F. Gazeau, and T. Pellegrino, *Chem. Mater.* **23**, 4170 (2011).

²¹B. Heinrich, A. Demund, and R. Szargan, *Phys. Status Solidi C* **4**(6), 1836 (2007).

²²M. T. Chang, L. J. Chou, C. H. Hsieh, Y. L. Chueh, Z. L. Wang, Y. Murakami, and D. Shindo, *Adv. Mater.* **19**, 2290 (2007).

²³H. Ohldag, A. Scholl, F. Nolting, E. Arenholz, S. Maat, A. T. Young, M. Carey, and J. Stohr, *Phys. Rev. Lett.* **91**, 017203 (2003).